Acta Astronautica 162 (2019) 497–510

Contents lists available at ScienceDirect

Acta Astronautica

journal homepage: www.elsevier.com/locate/actaastro

Calibration and preliminary tests of the Brine Observation Transition To Liquid Experiment on HABIT/ExoMars 2020 for demonstration of liquid water stability on Mars

Miracle Israel Nazarious[a,*], Abhilash Vakkada Ramachandran[a], Maria-Paz Zorzano[b,a], Javier Martin-Torres[a,c]

[a] Group of Atmospheric Science, Department of Computer Science, Electrical and Space Engineering, Luleå University of Technology, Luleå, Sweden
[b] Centro de Astrobiología (INTA-CSIC), Torrejon de Ardoz, Madrid, Spain
[c] Instituto Andaluz de Ciencias de la Tierra (UGR-CSIC), Armilla, Granada, Spain

ARTICLE INFO

Keywords:
Water on Mars
Deliquescence
Electrical conductivity
Instrument
ISRU
Mars exploration

ABSTRACT

The search for unequivocal proofs of liquid water on present day Mars is a prominent domain of research with implications on habitability and future Mars exploration. The HABIT (Habitability: Brines, Irradiation, and Temperature) instrument that will be on-board the ExoMars 2020 Surface Platform (ESA-IKI Roscosmos) will investigate the habitability of present day Mars, monitoring temperature, winds, dust conductivity, ultraviolet radiation and liquid water formation. One of the components of HABIT is the experiment BOTTLE (Brine Observation Transition To Liquid Experiment). The purposes of BOTTLE are to: (1) quantify the formation of transient liquid brines; (2) observe their stability over time under non-equilibrium conditions; and (3) serve as an In-Situ Resource Utilization (ISRU) technology demonstrator for water moisture capture. In this manuscript, we describe the calibration procedure of BOTTLE with standard concentrations of brines, the calibration function and the coefficients needed to interpret the observations on Mars.

BOTTLE consists of six containers: four of them are filled with different deliquescent salts that have been found on Mars (calcium-perchlorate, magnesium-perchlorate, calcium-chloride, and sodium-perchlorate); and two containers that are open to the air, to collect atmospheric dust. The salts are exposed to the Martian environment through a high efficiency particulate air (HEPA) filter (to comply with planetary protection protocols). The deliquescence process will be monitored by observing the changes in electrical conductivity (EC) in each container: dehydrated salts show low EC, hydrated salts show medium EC and, liquid brines show high EC values. We report and interpret the preliminary test results using the BOTTLE engineering model in representative conditions; and we discuss how this concept can be adapted to other exploration missions.

Our laboratory observations show that 1.2 g of anhydrous calcium-chloride captures about 3.7 g of liquid water as brine passing through various possible hydrate forms. This ISRU technology could potentially be the first attempt to understand the formation of transient liquid water on Mars and to develop self-sustaining in-situ water harvesting on Mars for future human and robotic missions.

Abbreviations: HABIT, HabitAbility: Brines, Irradiation, and temperature; BOTTLE, Brine Observation Transition To Liquid Experiment; ISRU, In-situ resource utilization; MSL, Mars science laboratory; GRS, Gamma Ray Spectrometer; RSL, Recurring slope lineae; DRH, Deliquescence relative humidity; ERH, Efflorescence relative humidity; CU, Container Unit; ATS, Air temperature sensor; EU, Electronic Unit; GTS, Ground temperature sensor; UVS, Ultraviolet sensor; HEPA, High efficiency particulate air; EC, Electrical conductivity; AC, Alternating current; MMS, Mojave Mars simulant

* Corresponding author.
E-mail addresses: miracle.israel.nazarious@ltu.se (M.I. Nazarious), abhilash.vakkada-ramachandran@ltu.se (A.V. Ramachandran), maria-paz.zorzano.mier@ltu.se (M.-P. Zorzano), javier.martin-torres@ltu.se (J. Martin-Torres).

https://doi.org/10.1016/j.actaastro.2019.06.026
Received 8 January 2019; Received in revised form 20 May 2019; Accepted 20 June 2019
Available online 22 June 2019

1. Introduction

1.1. Liquid water on Mars

Finding liquid water on present day Mars has implications on its habitability [1] and future human exploration [2,3]. Brines have been postulated to be produced on present day Mars under specific environmental conditions of temperature (T) and relative humidity (RH), in a diurnal absorption and evaporation cycle of atmospheric water vapor supported by the deliquescent chloride (Cl^-) and perchlorate (ClO_4^-) salts that exist on the surface of Mars [4].

The presence of these salts was detected by both the Phoenix Lander in the north polar plains and by the Curiosity rover/Mars Science Laboratory (MSL) at Gale Crater, on equatorial Mars. The in-situ analysis by the Phoenix Wet Chemistry Lab at the Phoenix landing site [5] confirmed the presence of magnesium or sodium-perchlorates and, calcium-perchlorate [6–8] was observed by the MSL mission at Gale. Viking data reanalysis suggested the presence of perchlorates in the shallow subsurface of Mars at its landing site [9]. Furthermore, chlorine is distributed globally on Mars as detected by the Mars Odyssey's Thermal Emission Imaging System (THEMIS) [10] and Gamma Ray Spectrometer (GRS) [11,12]. It has been recently demonstrated that plasma chemistry occurring during dust storms can actually be a source of formation for the large amount of perchlorates found on Mars [13]. This would mean that there is a continuous process for perchlorate formation and that they may be expected everywhere on the planet.

Chloride and perchlorate salts can form stable hydrates and liquid brines by absorbing atmospheric water vapor through deliquescence (transition from crystalline solid to aqueous solution) [14–23]. The local regolith-atmosphere coupling has been postulated to be a possible candidate for the seasonal occurrence of Recurring Slope Lineae (RSL) or slope streaks, frequently featured in the southern slopes of the equatorial Martian surface [24–30]. Other liquid related flow-like features like the low latitude slope streaks [31] and the Dust Dune Spots [32] were also claimed to be because of this water lubricated “wet” mechanism. Supporting the argument of this mechanism, the MSL measurements showed that the environmental conditions allowed for formation of night-time transient liquid brines in the uppermost 5 cm of the subsurface which then evaporate after sunrise [33]. Martin-Torres et al. [4] described the hypothetical diurnal water cycle for low latitude region on Mars representing the atmosphere–regolith water interchange [34,35]. The presence of liquid water on Mars if confirmed, could have potential impact on the chemistry and thereby the search for Martian life [36,37]. The purpose of the Brine Observation Transition To Liquid Experiment (BOTTLE) of the ExoMars surface platform is to have a controlled experiment with these salts to monitor their interaction with the atmosphere, investigating the processes of deliquescence, efflorescence, and the formation of liquid brines.

1.2. Deliquescence and efflorescence

Deliquescence is a phase transition from a crystalline solid to an aqueous solution that occurs at a specific condition, when the relative humidity (RH) is equal to or greater than the deliquescence relative humidity (DRH) of a salt and the temperature is within a certain range that depends on the salt phase diagram [38,39]. Efflorescence is the opposite; a phase transition from aqueous solution to a crystalline solid that occurs when the relative humidity (RH) is equal to or lesser than the efflorescence relative humidity (ERH) of a salt. The DRH and ERH values of the HABIT salts are summarized in Table 1.

At equilibrium, the water activity (a_w) of the brine formed can be related to the relative humidity as a_w = RH%/100 [42]. The deliquescence relative humidity (DRH) is thus estimated by the water activity over a saturated salt solution [43]. DRH and ERH for each salt vary as a function of temperature [44], with deliquescence occurring at temperatures as low as its eutectic point [42]. DRH increases with decreasing temperature (salts become less hygroscopic at lower temperatures), primarily because of the change in solubility [43].

Table 1
DRH and ERH values of BOTTLE salts. The temperatures mentioned alongside corresponds to the reported temperature limits at which the deliquescence and efflorescence values are valid for each salt.

Salt	DRH (%)	ERH (%)	Ref.
Anhydrous $Ca(ClO_4)_2$	13 at 273 K	1 at 273 K	[20]
$Mg(ClO_4)_2{\cdot}6H_2O$	42 at 273 K	19 at 223–273 K	[16]
$CaCl_2{\cdot}6H_2O$	29 at 298 K	3.5 at 273 K	[18,40,41]
Anhydrous $NaClO_4$	38 at 223–273 K	13 at 223–273 K	[16]

Salt solutions tend to supersaturate at RH < DRH when a metastable state is achieved due to kinetic limitations and exhibit hysteresis [16,20,38,45]. This hysteresis behaviour may allow liquid brine solutions to exist at low relative humidity, relevant to the Martian day [22] and this may explain the prolonged observation of the RSL. The efflorescence relative humidity (ERH) is lower than the DRH for most inorganic salts [38,46] because of the kinetic inhibition of salt crystallization in super cooled solutions [42].

1.3. Brine formation process

To illustrate the calibration procedure, we focus here on the brine formation process of anhydrous calcium-chloride. In equilibrium with the saturated solution, the solid phase of the $CaCl_2$-H_2O system is formed by ice on the low concentration side ($CaCl_2$ *wt%* = 0), by hydrates with 1/3, 1, 2, 4, and 6 mol of water per mole of salt as the salt concentration in the solution increases, and by anhydrous salt at the highest concentration ($CaCl_2$ *wt%* = 100) [47]. In principle, deliquescence will follow the path from anhydrous salt to liquid brine via transitions between different hydrate forms (one or more) while efflorescence follows the opposite path. Both deliquescence and efflorescence depend on the temperature and relative humidity of the environment that the salt is interacting with. The solid-liquid phase diagram of the $CaCl_2$-H_2O system, thus consists of branches corresponding to the particular hydrates separated either by an eutectic (198.15 K for $Ca(ClO_4)_2$, 216.15 K for $Mg(ClO_4)_2$, 223.05 K for $CaCl_2$, 236 K for $NaClO_4$) or by a peritectic point (at transition points of different hydrate forms), where two solids are precipitating simultaneously [43].

The brine formation process for some Mars-relevant perchlorates have already been studied detecting the changes in phase or hydration state of individual salt particles [17,38,42] with Raman microscopy [16,22,48–50]. Different studies have described the formation of frozen brine under Mars-relevant conditions [49–51]. The clear demonstration of the existence of transient liquid water on Mars has been elusive and is one of the main purposes of BOTTLE/HABIT. While with HABIT we expect to monitor the brine formation process of the pure hygroscopic salts contained in the BOTTLE cells, on the surface of Mars, these salts exist as a mixture with the regolith. But studies have suggested that the hypothesized phenomenon of liquid brine formation holds true both in pure salt form and in mixture with regolith grains [50,52].

1.4. Electrical conductivity

Heinz et al. [40], demonstrated that the electrical conductivity is an excellent parameter to monitor the deliquescence process of salts. The electrical conductivity measurements correlated well with the deliquescence rates of soil-salt mixtures (they used as Martian analogue soil, a mixture of JSC Mars-1a and perchlorates or chlorides) and provided an overall characterization in terms of time series of the brine formation process, which seems more sensitive than either Raman spectroscopy or estimates based on deliquescence relative humidity [40]. This technique has been commonly used for detection of liquid or

frozen water in soils [53,54].

But the deliquescence and efflorescence behaviour of the salts, and thus the brine formation process have not yet been quantified in terms of the different hydrate forms, as a function of electrical conductivity and for the specific configuration of the BOTTLE instrument.

In this manuscript, we present the calibration procedure of BOTTLE and interpret the preliminary test results as an analogue to the observations on Mars and its implications while highlighting some of the features of the instrument from the operation point of view. In section 2 we describe BOTTLE sample preparation and experimental setup. In section 3 we focus on establishing a relation between electrical conductivity, water cycle and the brine formation process, with appropriate relevance to hydrate forms and the transition regions of the system. In section 4 we demonstrate the validity of the calibration model with calcium-chloride ($CaCl_2$) as an example. Our future plans are described in section 5; and we present our conclusions and implications in section 6.

2. Material and methods

2.1. The instrument

BOTTLE is one of the modules of the HABIT/ExoMars 2020 Surface Platform (ESA-IKI Roscosmos). Fig. 1 shows the engineering model of HABIT, including BOTTLE.

BOTTLE consists of four containers with deliquescent salts that have been found on Mars (calcium-perchlorate $Ca(ClO_4)_2$, magnesium-perchlorate $Mg(ClO_4)_2$, calcium-chloride $CaCl_2$ and sodium-perchlorate $NaClO_4$) and two containers that are open to the air, to collect atmospheric dust. The salts are exposed to the Martian environment through a High Efficiency Particulate Air (HEPA) filter (to comply with planetary protection protocols). The deliquescence process of salts will be monitored by observing the changes in electrical conductivity (EC) in each container with three levels of electrode pairs. It is also equipped with a PT1000 temperature sensor to provide reference to brine temperature during measurement and a heater to allow recyclability of salts if required. With BOTTLE, we expect to identify the phase changes from dry salt to its hydrate forms, to liquid brine or to frozen brine. HABIT will be set to operate for the first 5 min of every hour at a measuring frequency of 1000 ms accounting for 300 data points per hour.

2.2. Sample preparation

The samples used for this work were derived from anhydrous $CaCl_2$ salt in fine powder form, purchased from Merck KGaA (98% pure, CAS-No: 10043-52-4). The homogeneous solutions of different $CaCl_2$ *wt*% of 0% (water only) to 100% (anhydrous salt only) with 10% increments were prepared by adding appropriate amount of water to anhydrous $CaCl_2$.

For experiments with $CaCl_2$ *wt*% of 40%, 50%, 60%, 70%, 80%, 90% and 100%, we used 2 g of anhydrous $CaCl_2$ in each of the six BOTTLE containers. Salt was weighed on a weighing scale (Pioneer OHAUS, 0–200 g) and a micropipette (VWR EHP Pipettor, Single Channel, 60–1000 µl) was used to accurately measure the amount of water added. The overall volume of the mixture for these experiments were until mid-electrodes in each cell. The prepared mixture was left for about 5–10 min to reach equilibrium before the experiment. For the experiments, a set of solutions with $CaCl_2$ *wt*% of 0%, 10%, 20% and 30%, were previously prepared and added into BOTTLE until the high electrode.

2.3. Experimental setup

The experiments were conducted in a climatic chamber (Heraeus HT 4010, 233 K–453 K) at Martian equivalent temperatures decreasing between 298.16 K and 228.16 K at $\Delta T = 2.63$ K/min which was the normal operational sweeping rate of the chamber. The RH of the environment was pumped from the ambient laboratory conditions and was measured using a temperature and humidity data logger (Maxim Integrated DS1923-F5# Hygrochron, T: 253 K–358 K, RH: 0%–100%). BOTTLE was placed inside the chamber while the Electronics Unit (EU) was left at ambient laboratory temperature (to avoid any thermal noise, since the electronics of the engineering model was not representative of the flight model and is thus not designed for low temperatures). The cables connecting the EU and BOTTLE pass through the port on the side of the chamber. We performed experiments on two timescales.

We performed first experiments with variable salt wt%, these were long and slow experiments to probe the equilibrium or near-equilibrium processes between salt and water vapor at constant temperature. Here, the water *wt*% was gradually decreased with sufficient time between water additions to allow for equilibrium to be reached between the salt and the atmosphere. This experiment targeted to observe the

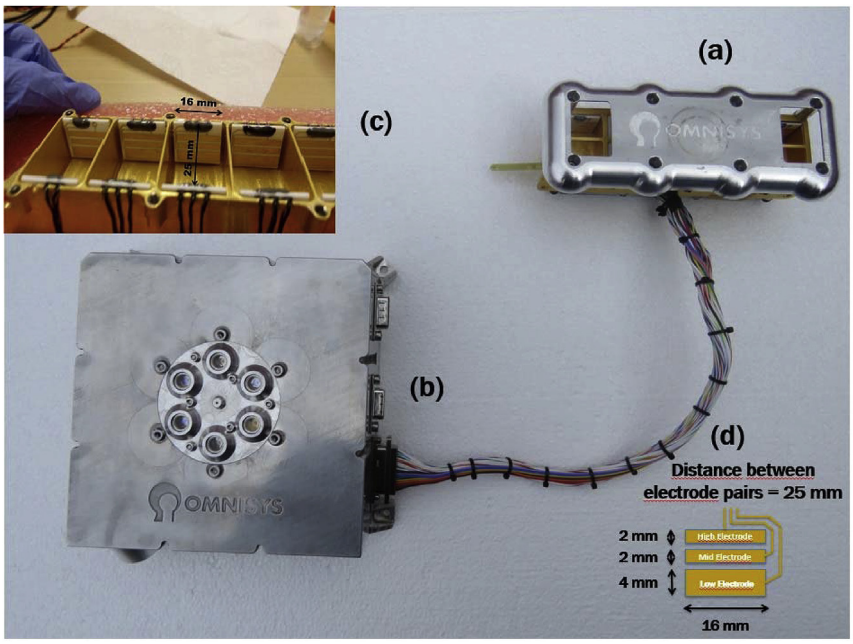

Fig. 1. Image of the HABIT instrument. (a) Container Unit (CU) hosting BOTTLE and the Air Temperature Sensor (ATS), (b) Electronic Unit (EU) hosting the Ground Temperature Sensor (GTS) and the Ultraviolet Sensor (UVS), (c) Interior of BOTTLE and view of the electrodes, (d) Details of the electrode configuration showing the geometrical dimensions of the low, mid and high electrodes (in mm) and the distance between the electrode pairs positioned between the walls of each BOTTLE cell. The dimensions are used for evaluating the geometrical cell constant of each electrode pair.

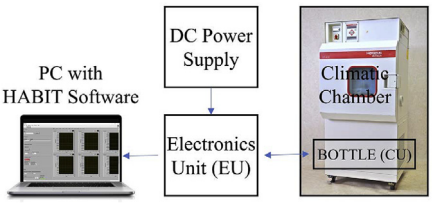

Fig. 2. Experimental setup showing different control blocks, the climatic chamber and the HABIT graphical user interface.

temperature dependence in brine with different salt concentrations. We then performed experiments with variable temperature conditions, these were short and fast experiments at constant salt *wt*%. This second type of experiment was focussed on evaluating the impact on the instrument measurements of kinetic factors of the brine that are associated with temperature including the brine freezing.

Gough et al. [42] reported that an equilibrium between the sample and the atmospheric water vapor was reached in both the short and long timescale experiments (suggested by the lack of difference in DRH for short vs long timescale experiments) and that it is not necessary to closely monitor timescales. To simplify the experimental setup and shorten the experiment duration, we performed variable temperature experiments with constant $CaCl_2$ wt% samples. Our calibration experiments used the prepared $CaCl_2$ brine of different concentrations to monitor their electrical conductivity measurements at different temperatures rather than observing the entire slow deliquescence process. The block diagram of the experimental setup used is shown in Fig. 2.

2.4. Outdoor experiments

We performed an outdoor operation of the HABIT instrument in the arctic environmental conditions of Luleå, Sweden, to mimic the operation under naturally varying, uncontrolled, planetary environmental conditions. For this demonstration, we used samples including different amounts of calcium-chloride and the two different *wt*% mixtures of Mars regolith simulant (MMS-1 Mojave Mars Simulant, Fine Grade, The Martian Garden) and calcium-chloride. The experiment was monitoring for the brine formation process in each of the six cells of BOTTLE containing different samples. Data were collected for the first 5 min of every hour at a measuring frequency of 1000 ms accounting for 300 data points per hour. The experiment was run for 10 days to observe the liquid brine formation process and to represent the EC method used by BOTTLE to track the changes in salt hydrate forms unequivocally.

In parallel, we also performed two more outdoor experiments to obtain an estimate of the amount of water captured and released by $CaCl_2$ and quantify the brine formation process by weight. For one experiment, we used a sample of 1.2 g of anhydrous $CaCl_2$ prepared in a petri dish. For the other experiment, we used a mixture of 1.2 g Mars regolith simulant (MMS-1 Mojave Mars Simulant, Fine Grade, The Martian Garden) and 20% anhydrous $CaCl_2$ (0.3 g). These experiments were exposed to the arctic climatic conditions of Luleå, Sweden for 3 days. Images were taken and the petri dish with samples were weighed at noon every day. The environmental conditions during these days varied between 268.16 K and 273.16 K for T, and 68% and 88% for RH.

3. Theory and calculation

3.1. Measurements, data sampling and data treatment

BOTTLE measures the current flow, *I* and the voltage drop, *V* across low, mid and high electrode pairs (see Fig. 1c and d) of each of the six containers, along with its temperature. Consequently, the conductance, *G* in Siemens is calculated with equation (1).

$$G = \frac{I}{V}(S) \tag{1}$$

Ambient laboratory experiments for evaluating the coefficients of the calibration function were performed for 100 data points at a frequency of 1000 ms. For the experiments of variable temperature with $CaCl_2$ *wt*% = 40%, 50%, 60%, 70%, 80%, 90% and 100%, the data was collected during a temperature sweep from 298.16 K to 228.16 K with the CU in the climatic chamber at a frequency of 1000 ms. For experiments with $CaCl_2$ *wt*% = 0%, 10%, 20% and 30%, 100 data points each were collected at a frequency of 1000 ms between temperatures of 298.16 K and 228.16 K while making measurements at every 5 K decrements (298.16 K, 293.16 K, 288.16 K …, 228.16 K). The measurement of the zero offset (or dry calibration experiment) was conducted in the laboratory ambient temperature at the same frequency.

3.2. Calibration model

The primary goals of the BOTTLE calibration procedure were: 1) to establish a relationship between the electrical conductivity and salt hydrate, brine or frozen forms and; 2) monitor and detect unequivocally the liquid brine formation process with special emphasis on phase transitions. The following factors are considered for the calibration model.

3.2.1. Zero offset or dry calibration

The zero offset of an instrument is normally used to determine the null reference of the experimental case. Here, we determine the conductivity of empty containers with just the natural noise frequency of the instrument electronics. The measured zero offset provides the first point (dry) of the calibration function.

3.2.2. Geometrical cell constant, K_{cell}

The measured conductance of the sample is translated to electrical conductivity by multiplying with the geometrical cell constant of the electrode pair, K_{cell} as in equation (2).

$$\sigma_{measured} = K_{cell} \times G(\mu Scm^{-1}) \tag{2}$$

The geometrical cell constant of the electrode pair depends on its physical dimensions. There are three electrode pairs each in four middle containers and two electrode pairs each in the two end containers summing to a total of 16 electrode pairs and consequently 16 geometrical cell constants are to be calculated with equation (3).

$$K_{cell} = \frac{Distance\ between\ electrodes\ (in\ cm)}{Surface\ area\ of\ electrodes\ (in\ cm^2)} = \frac{d}{A} \tag{3}$$

where,

$d = 2.5\ cm$
$A_{low} = 1.6\ cm \times 0.4\ cm = 0.64\ cm^2$
$A_{mid} = 1.6\ cm \times 0.2\ cm = 0.32\ cm^2$
$A_{high} = 1.6\ cm \times 0.2\ cm = 0.32\ cm^2$

We assume the symmetrical construction of BOTTLE electrodes and the distance between each of the electrode pairs are the same.

Therefore, $K_{cell,low} = 2.5\ cm/0.64\ cm^2 = 3.9062\ cm^{-1}$

$K_{cell,mid} = 2.5\ cm/0.32\ cm^2 = 7.8125\ cm^{-1}$
$K_{cell,\ high} = 2.5\ cm/0.32\ cm^2 = 7.8125\ cm^{-1}$

Note: Subscripts *low*, *mid* and *high* denote low, mid and high electrode pairs.

3.2.3. Calibration function and coefficients

For correcting the inaccuracy in geometrical cell constants of the electrode pair and cancelling the offset in the instrument electronics, a

Table 2
Coefficients of the polynomial equation (4) for all electrode pairs: dry, 1413 μScm^{-1} and 5000 μScm^{-1}.

Electrode	a_2	a_1	a_0
Cell-1 Low	3.9406e-04	−0.5096	0.028
Cell-2 Low	3.761e-04	−0.4539	1.2855
Cell-3 Low	8.7548e-05	0.5955	−0.2963
Cell-4 Low	9.598e-04	−1.7777	0.2552
Cell-5 Low	2.0289e-04	−0.2291	0.0954
Cell-6 Low	3.3811e-04	−0.5392	0.0132
Cell-1 Mid	−2.5e-03	8.9899	1.2948
Cell-2 Mid	−4.9485e-04	3.1952	−15.7486
Cell-3 Mid	−2.2e-03	8.1604	−3.5737
Cell-4 Mid	1.7e-03	−6.259	1.6429
Cell-5 Mid	−2.1e-03	9.6591	−4.4231
Cell-6 Mid	−2.4e-03	8.2325	−0.2747
Cell-2 High	−6.0406e-04	3.5071	−9.4149
Cell-3 High	−2.9e-03	9.2806	−13.9164
Cell-4 High	1.0776e-04	0.2762	−0.1138
Cell-5 High	4.0185e-04	−1.3571	1.4615

calibration function was determined with two conductivity standards: 1413 μScm^{-1} and 5000 μScm^{-1} respectively, with a least square regression, by fitting a 2nd order polynomial curve as in equation (4). The two calibration standards were chosen such that their electrical conductivity values allow for an optimal fitting within the full range 0 μScm^{-1} to 5000 μScm^{-1}, to cover the expected range of conductivities of HABIT. This procedure is termed as two-point calibration (including dry point). The specific choice of the calibration standards is chosen depending on the required accuracy within a certain measurement range. The flight model of the instrument will be calibrated, following this same procedure, with several calibration standards of various electrical conductivity values to allow for better accuracy within various narrower measurement ranges of particular interest.

$$\sigma_{actual} = a_2\sigma^2_{measured} + a_1\sigma_{measured} + a_0 \ (\mu Scm^{-1}) \tag{4}$$

The obtained calibration function coefficients are summarized in Table 2, for each of the six cells and for the three electrodes in each cell (low, mid and high). The differences in the coefficients between each electrode and cell may be attributed to the difference in their physical dimensions (see Fig. 1d) and the asymmetry in the electrode configuration.

This way, we have obtained 16 sets of calibration function coefficients, where each set corresponds to one range of conductivity for one electrode pair. The two-point calibration is normally sufficient for accurately converting the raw data to actual conductivity measurements. But, the order of the polynomial can be increased with more conductivity standard points for greater accuracy in specific ranges.

3.2.4. Temperature vs electrical conductivity

Electrical conductivity is dependent on temperature as expressed in equation (5) and thus usually the measured electrical conductivity at various temperatures should be reported corresponding to a standard temperature (298 K) considering an arbitrary constant (assuming a linear electrical conductivity-temperature relation) for temperature compensation.

$$\sigma = f(T) \tag{5}$$

However, when working with brines at Martian temperatures between 228.16 K and 298.16 K, the electrical conductivity-temperature relation gets complicated especially below the freezing point of the brine because of the non-linearity in the electrical conductivity-temperature relation of the frozen brine. Thus, we refer to electrical conductivity only as an indication of the hydrate form for a given salt *wt*% (and to determine the DRH) to track the main phase transitions under Martian conditions rather than to have an absolute reference of EC comparable with our standard laboratory temperatures. Therefore, we do not apply the temperature compensation for the measured electrical conductivity but rather use it directly to determine the hydration state of the salt while using the temperature reference to provide context for a better interpretation of the temperature-related fluctuations in the electrical conductivity and to estimate the point where the brine freezes.

3.2.5. Electrical conductivity vs hydrate form

The core result of this work is to determine the relation between electrical conductivity and hydrate form of the brine at different temperatures as expressed in equation (6).

$$\sigma = f(x,\ T) \tag{6}$$

The hydrate form of the brine depends on the mole fraction of salt in the brine and the temperature. Mole fraction (x) and mass fraction ($w = wt\%/100$) are related as in equation (7).

$$x_{CaCl2} = \frac{\frac{w_{CaCl2}}{M_{CaCl2}}}{\frac{w_{CaCl2}}{M_{CaCl2}} + \frac{(1 - w_{CaCl2})}{M_{H2O}}} \tag{7}$$

where,

w_{CaCl2} – Mass fraction of $CaCl_2$ in the solution
w_{H2O} – Mass fraction of H_2O in the solution
M_{CaCl2} – Molar mass of $CaCl_2$ = 110.98 g/mol
M_{H2O} – Molar mass of H_2O = 18.01528 g/mol

3.2.6. Electrode degradation

With the constant exposure of the electrode material to brine with an alternating current (AC), the electrodes might corrode through the operational lifetime of the instrument which is expected to be one Earth year. We have observed some corrosion in the platinum electrodes of the BOTTLE engineering model during the laboratory and field-site operation in the first six months. Although the flight model of BOTTLE has gold electrodes which are more resistant to corrosion, it is part of the calibration procedure to be able to interpret the signs of degradation of the electrodes. The fraction of corroded electrode area will not contribute as the unperturbed platinum surface to the electrical conductivity measurement. Thus, eventually, an extended corrosion may affect the measurements. The rate of corrosion of the electrodes can be characterized with laboratory experiments but for data reliability purposes, in the event of corrosion during the operation of BOTTLE/HABIT on Mars, we strategize to: 1) reset the instrument hardware by heating up the salt and allow it to lose any captured water and then; 2) take a null measurement of the anhydrous salt before proceeding with the experiment. Our laboratory experiments showed that it took about 7200 s at 328.15 K (see also section 4.4) to dehydrate the saturated $CaCl_2$ brine at a laboratory ambient RH of ~20%. As an effort to mitigate the corrosion, the exposure of the current to the electrodes could be limited which requires a revised scheduling plan for making less frequent measurements. In the worst case, the data provided will contain an error bar with a specified uncertainty. We have noticed from our experiments that the corrosion in the electrode induced unstable electrical conductivity measurements that deviates higher or lower than the mean measurements within a set of data recorded continuously over a short period. Thus, the uncertainty limits in the measurements will be estimated from the deviation in the electrical conductivity within each scheduled measurement of 5 min (see section 2.1). We will work on the corresponding calibration to mitigate the errors due to corrosion in the future as described in section 5.

3.2.7. Other factors

Salt granularity, salt compactness, brine distribution, salt depth, and electronic noise also contribute to the measured electrical conductivity and it is important to base the interpretation considering these factors. This work gives only the basic information about these aspects, but

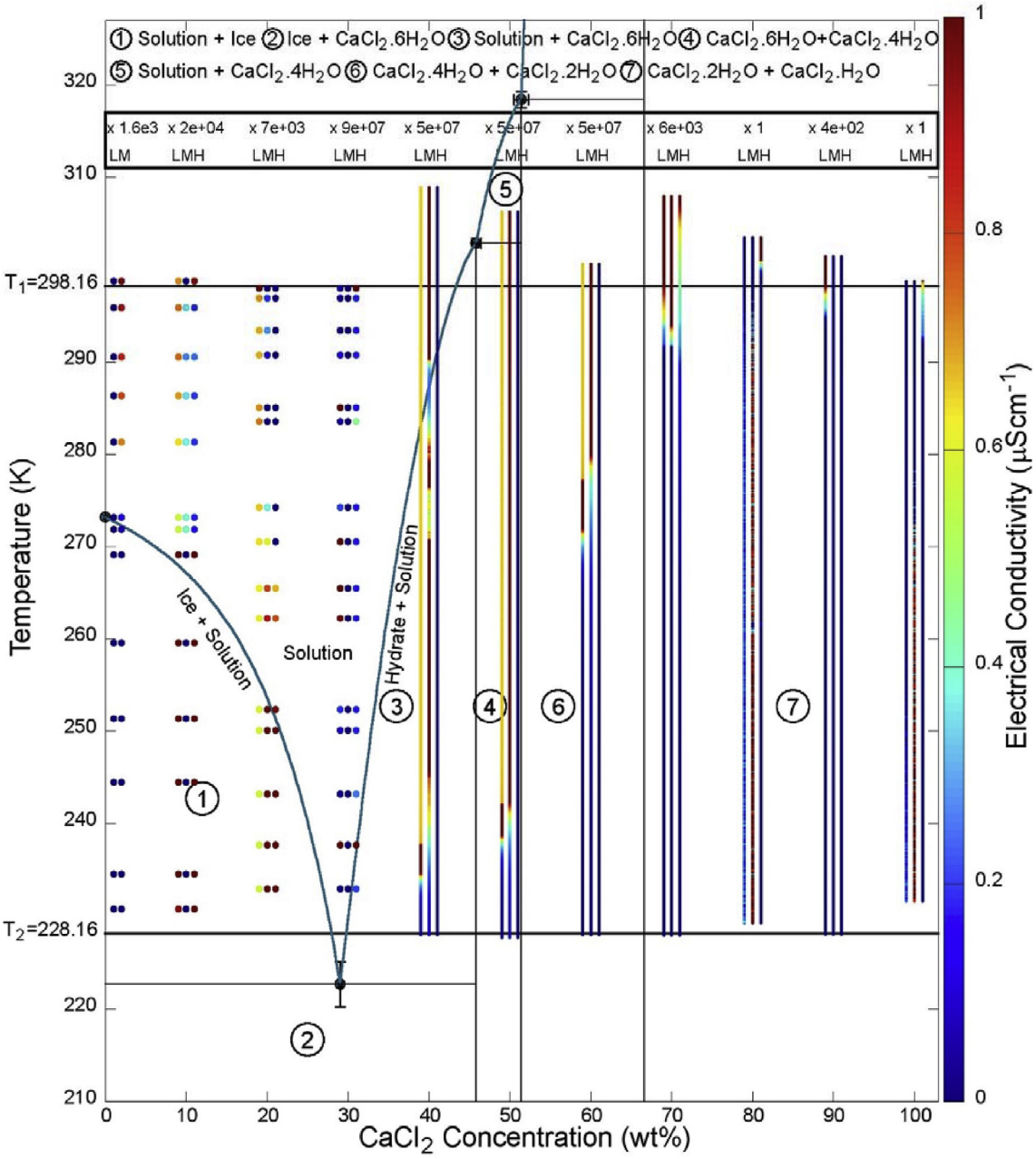

Fig. 3. Calcium-chloride – Water binary system solid-liquid equilibrium phase diagram. Overlaid with EC (in μScm^{-1}) measurements from the variable temperature experiments with different salt *wt*%. The three (or two) vertical lines or points with color code at salt *wt*% = 100, 90 … 0 shows the EC ranges for different salt hydrate forms at three levels of electrodes (of Cell-4 in BOTTLE) denoted by L for Low, M for Mid and H for High electrodes. The corresponding multiplier scaling factor for each experimental wt% is indicated above (in the box). This factor must be multiplied to the EC values indicated in colour, following the bar on the right. Each multiplier scaling factor is common to the three electrodes (L, M and H). A different multiplier scaling factor was fixed for each salt *wt*% experiment to allow for clear distinction of small EC changes with the phase diagram. This also shows a trend with higher factors at $CaCl_2$ concentration of 30%, which is consistent with the highest EC values recorded for the brine with salt *wt*% = 30. Since the quantity of initial samples were chosen to only fill until the mid-electrode, only the EC values corresponding to low and mid electrodes are relevant in terms of comparison of EC range. The curves were calculated from the empirical model developed by Patek et al. [47], describing the T-*x* relation from the historical experimental data. Here, the molar fraction (*x*) was translated to *wt*% (=*w**100) with equation (7). The regions 1 to 7 indicated with the circled numbers denote the various forms of the $CaCl_2$ – H_2O system including ice, solution, hydrates and their mixtures. The error bars at the eutectic and peritectic points are shown three times larger in magnitude for a better visibility. (For interpretation of the references to colour in this figure legend, the reader is referred to the Web version of this article.)

careful consideration is reserved for future work as described in section 5.

4. Results and discussion

4.1. $CaCl_2$ – H_2O system phase diagram highlighting EC

The results of the variable temperature experiments with samples of different salt *wt*% (corresponding to different salt hydrate forms) are shown in Fig. 3. We observed the interrelation between electrical

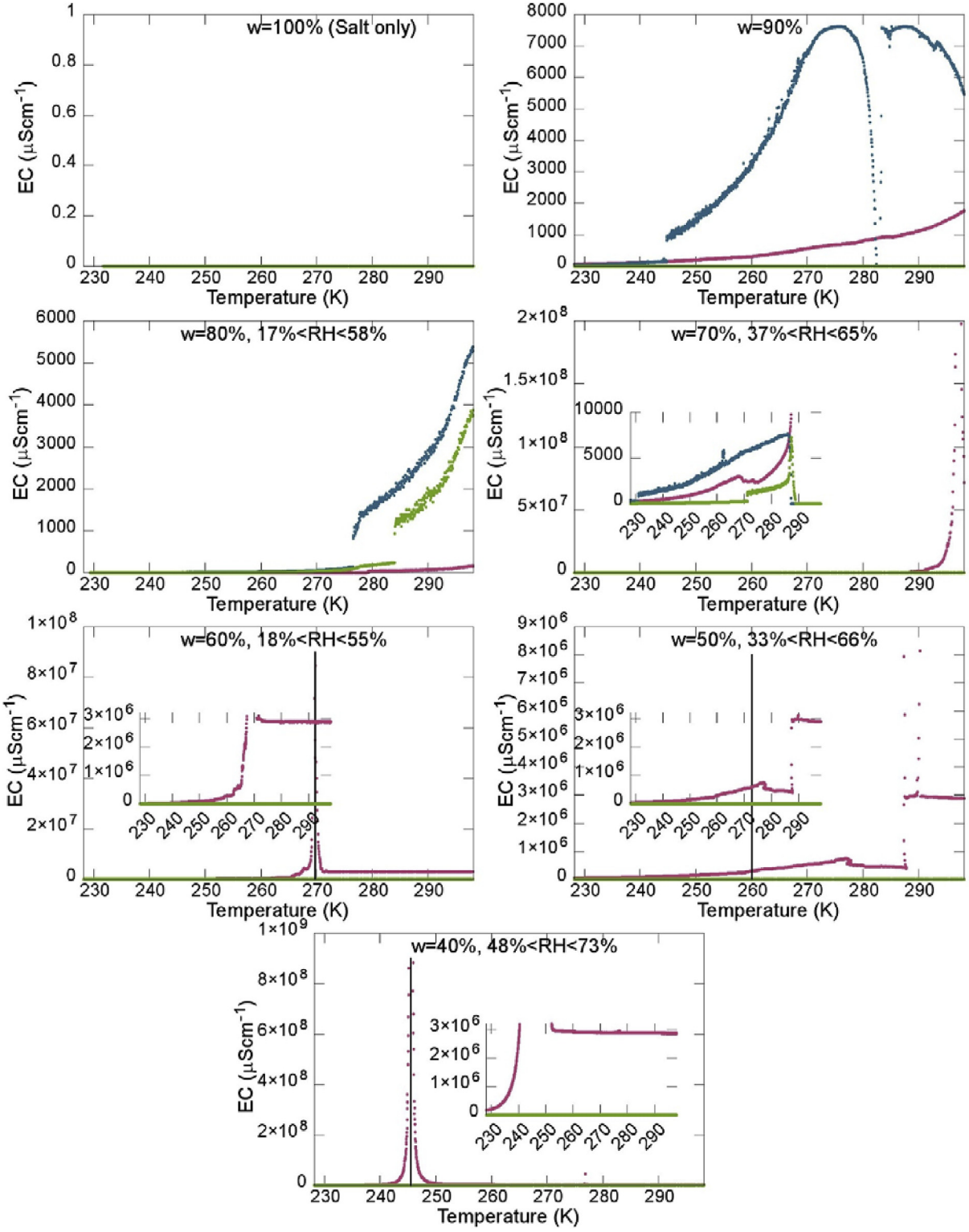

Fig. 4. Variable temperature calibration experiments in Cell-3 when the temperature is decreased from 298.16 K to 228.16 K. Each graph shows the changes in electrical conductivity (Y-axis; in μScm^{-1}) as a function of temperature (X-axis; in K) for samples of different salt *wt*% (= 100, 90 … 40). These results were from the low (red), mid (blue) and high (green) electrodes experimental data of Cell-3 in BOTTLE. The inset plots are provided to better visualize the EC ranges of different cases. The data from the mid electrode was removed from the plot for experiments with salt *wt*% = 70, 60, 50 and 40 because of corrupted EC values. The relative humidity (%) during the experiments are indicated in the format: RH_{min} < RH < RH_{max}, where the RH_{min} occurred at higher temperatures and RH_{max} at lower temperatures. The black vertical lines indicate the freezing point of the brine. (For interpretation of the references to colour in this figure legend, the reader is referred to the Web version of this article.)

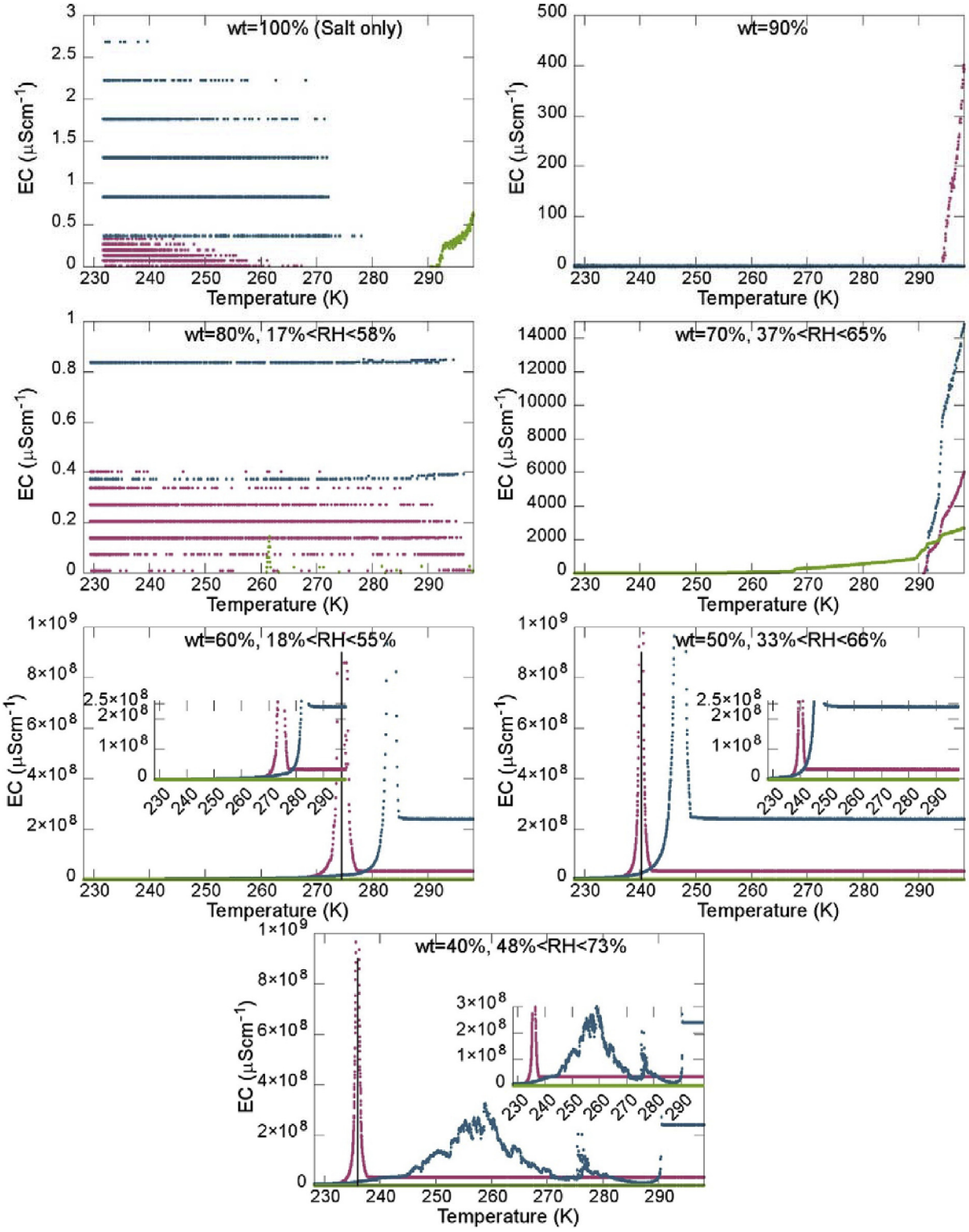

Fig. 5. Variable temperature calibration experiments in Cell-4 when the temperature is decreased from 298.16 K to 228.16 K. Each graph shows the changes in electrical conductivity (Y-axis; in μScm^{-1}) as a function of temperature (X-axis; in K) for samples of different salt *wt*%(= 100, 90 … 40). These results were from the low (red), mid (blue) and high (green) electrodes experimental data of Cell-4 in BOTTLE. The inset plots are provided to better visualize the EC ranges of different cases. The relative humidity (%) during the experiments are mentioned in the format: $RH_{min} < RH < RH_{max}$, where the RH_{min} occurred at higher temperatures and RH_{max} at lower temperatures. The black vertical lines indicate the freezing point of the brine. (For interpretation of the references to colour in this figure legend, the reader is referred to the Web version of this article.)

conductivity, temperature and salt *wt*% in terms of three main correlations: i) temperature dependence of electrical conductivity; ii) electrical conductivity ranges of different salt *wt*% samples; and iii) behaviour of different salt *wt*% samples at different temperatures with emphasis on liquid brine freezing.

Figs. 4 and 5 (different BOTTLE cells) show that, samples with

higher salt *wt*% (100, 90, 80 and 70) had either no measurable EC or extremely low EC values. This denotes a negligible or inexistent content of water in the salt between the electrodes (depending on brine distribution). Upon water addition, the anhydrous $CaCl_2$ formed hydrates that have a higher EC than the dehydrated salt (~ 0 μScm^{-1}). The maximum EC value of the first observed stable hydrate corresponds to the dihydrates of $CaCl_2$ (the first possible hydrates at these experiment temperatures, $\sim 1.5e+04$ μScm^{-1} for *wt*% = 70). Throughout the experiment, the temperature and EC followed a direct non-linear relation, mirrored with a decrease in the EC towards zero under colder temperatures. The EC values of liquid brine solution (~ 0.8–1^{*} $5e+07$ μScm^{-1}) were obtained already with *wt*% of 60% and at lower temperatures than predicted by the model. The shape of the theoretical phase diagram seems to underestimate the region where liquid state may appear. Also, samples with lower salt *wt*% (60, 50 and 40), showed stable and higher EC values until they exhibited an unexpected rise and fall in the EC (this will be denoted as EC spike in the rest of the paper), at the temperature that corresponds to the transition to frozen brine.

This change in behaviour is attributed to the temperature at which liquid brine freezing begins. Quantitatively, the EC spike of $\sim 1e+09$ μScm^{-1} was registered in the order up to 25 (higher) in magnitude for low electrode and 4 (higher) in magnitude for mid electrode. Furthermore, the EC spike for the low electrode occurs at a temperature colder than that of the mid electrode, explaining that the brine freezing originates at the upper surface of the brine and propagates downwards. Following this, the EC decreased towards zero until the completion of brine freezing.

The highest EC values of $CaCl_2$ brine was registered for samples of salt *wt*% = 30, of $\sim 9e+07$ μScm^{-1} (in close correspondence with the literature [55,56]) which exponentially reduced with lower salt *wt*% of 20%, 10% and 0%.

The inconsistency in the results of Cell-3 and Cell-4 for higher salt *wt* % samples is due to the inhomogeneity in the water distribution within the salt. On the contrary, the samples with lower salt *wt*% were easily homogenized after a thorough mixing. However, in real application on Mars, the situation will be similar to the former case and thus brine distribution (depending on salt granularity and salt compactness) is an important aspect to consider when understanding these EC measurements.

4.2. Outdoor operation and interpretation

This experiment constitutes the final step of the BOTTLE/HABIT calibration procedure. The results of the outdoor operation demonstration under the arctic environmental conditions of Luleå, Sweden during December 2017 are shown in Fig. 6.

The deliquescence process of different amount of calcium-chloride and the two different *wt*% mixtures of Mars regolith simulant and calcium-chloride were closely monitored with electrical conductivity measurements. During the experiment the environmental conditions varied naturally between: $261.46\,K < T < 279.9\,K$ and $50\% < RH < 100\%$. These conditions were favourable for $CaCl_2$ deliquescence and hence all the six containers showed the effect of deliquescence with different ranges in EC values. The range of EC values representing the hydrates and transient brine (maximum of ~ 140 μScm^{-1}) during this experiment was lower than the calibration experiments by several orders of magnitude because of the inhomogeneity in the brine distribution and the freezing temperatures at which the experiment was conducted. The moisture absorbed by the salt exhibited an uncontrolled distribution both horizontally and vertically wetting and dissolving some parts of the salt matrix and creating small voids that sometimes led to improper electrical contact of the salts with the electrode pairs. Also, at the very low sustained arctic winter temperatures, the salts rapidly froze into a compact physical structure with the initial water intake and did not form a free-flowing brine, as opposed to a loose powder salt structure and the formation of the free-flowing brine as seen in ambient calibration experiments.

We use the BOTTLE calibration results obtained earlier to account for a detailed interpretation of the liquid brine formation process in Cell-5 during the outdoor demonstration. This experiment is a demonstration of the BOTTLE nominal operation mode on Mars.

Print Version: Fig. 7 shows the different stages (Start, A, B, C, D, E, F, G, H) of the brine formation process segmented into transition points and regions between them.

E-Version: Video 1 shows the time-lapse animation of different stages (Start, A, B, C, D, E, F, G, H) of the brine formation process segmented into transition points and regions between them.

Supplementary video related to this article can be found at https://doi.org/10.1016/j.actaastro.2019.06.026.

The Cell-5 was filled with anhydrous $CaCl_2$ in fine powder form creating a salt matrix until the mid-electrode at the start of the experiment. The region between 'Start' and 'A' represents the dry anhydrous $CaCl_2$ with complete absence of water as marked by no measurable EC (~ 0 μScm^{-1}). $CaCl_2$ deliquescence began at the upper surface of the salt since this part was in direct contact with the atmospheric moisture, thus showing signs of increase in EC at the mid electrode first at 'A' after about 38 h (~ 1.6 days) from the start of the experiment (see Supplementary Fig. 1). Due to the exothermicity nature of this process which releases heat upon addition of water to the salt, a sudden increment in temperature of up to 5.2 K was also noticed. The water absorbed by the upper surface of the salt then penetrated downwards dissolving the salt and passing down the moisture towards the low electrode which registered an increasing EC at 'B' about 2 h (~ 1.7 days) later. The continuous growth in blue and red EC curves attribute to the continuous absorption of atmospheric moisture forming hydrates in the upper surface and penetration of the water downwards. The water accumulated over the hydrates then formed a thin brine pool on the upper surface that connected the high electrodes showing an EC signal (green curve) at 'C' after about 46 h (~ 1.9 days) which was also mirrored by a further growth (~ 80 μScm^{-1}) in the blue curve. The fluctuations in blue and green curves since then are caused by the continuous water absorption and varying temperatures, while the red line kept on growing with more water penetrating deep into the salt matrix and distributing within.

As the salt matrix absorbed more and more water, the volume of the salt hydrates formed decreased, up to finally dissolving the salt, lowering the level of the upper surface (decrease in height). The gradual lowering of the level was seen first at the high electrode as indicated by the fall of the green curve at 'D' after about 87 h (~ 3.7 days). The region between 'A' and 'D' resulted in the formation of the stable dihydrate of $CaCl_2$ (the first possible hydrates at these experiment temperatures). Since 'D', where the salt level was completely below the high electrode, the brine formation process continued as highlighted in the low and mid electrode EC values in the regions between 'B' - 'E' and 'A' - 'F' respectively, showing signs of transient brine with EC values as high as ~ 140 μScm^{-1}. Additionally, the associated temperature increase induced an EC change that recovered once the temperature equilibrium was achieved in the region between 'E' and 'G'. Because of further shrinkage in volume with formation of subsequent hydrate forms, the level of brine started to lower further at 'F' as indicated by the fall in blue curve after about 172 h (~ 7.2 days).

Now all the brine formed was accumulated only in the low electrode, thus registering near zero EC values at mid and high electrodes. As the brine freezing temperatures dominated, the transition to frozen brine occurred at 'G' after about 214 h (~ 9 days), as indicated by a sudden EC increase with the EC spike (~ 375 μScm^{-1}) at 'H' after 237 h (~ 9.9 days) from the start of the experiment. We observed this sudden rise and fall of EC at the temperature of brine freezing during the calibration experiments, but the EC spike here was comparatively slower and took about a day because of the low rate of change in temperature in contrary to a rapid $\Delta T = 2.6$ K/min during calibration experiments. As a result, we don't expect to observe a sharp peak in the BOTTLE

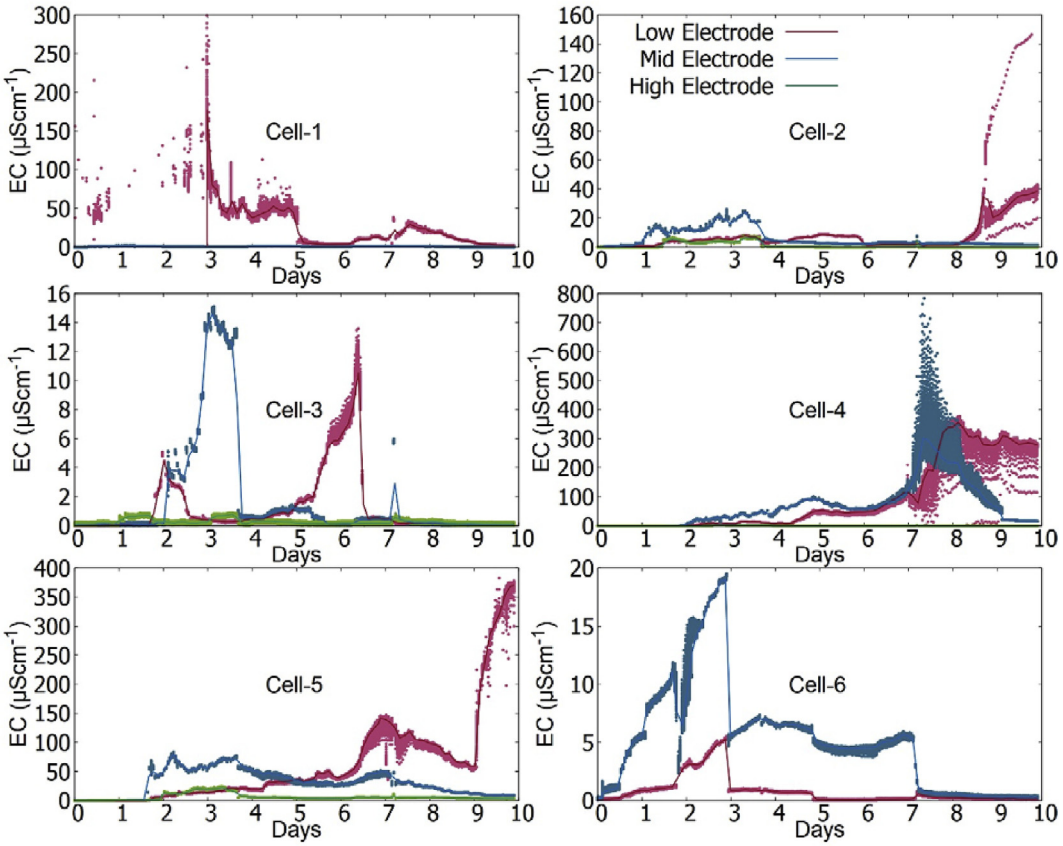

Fig. 6. BOTTLE/HABIT outdoor test in the Arctic region. Demonstration of BOTTLE/HABIT Engineering Model operation outdoors in Luleå, Sweden, showing deliquescence over time with transitions to hydrate forms and different phases of brine formation process. The legends mentioned on the top right subplot are common for all the subplots in the figure. Cell-1 contains Mars regolith simulant with 0.5% anhydrous $CaCl_2$ filled to low electrode (2.027 g); Cell-2 and Cell-3 contains 1.2 g of anhydrous $CaCl_2$ filled to low electrode; Cell-4 and Cell-5 contains 2 g of anhydrous $CaCl_2$ filled to mid-electrode; Cell-6 contains Mars regolith simulant with 1.85% anhydrous $CaCl_2$ filled to low electrode (5.01 g).

outdoor experiments to signify the brine freezing but a gradual increase in EC to a value that is several orders of magnitude higher than the normal experiment progression during the formation of the brine. The series of different stages of the experiment is summarized in Table 3.

The exothermic footprint was consistent with a temperature increase of up to 5.2 K at initial water absorption and up to 2.5 K at subsequent transitions associated with the formation of hydrates and transient brine as seen in the orange curve. This exothermic behaviour directly influences the EC values as we have seen from the outdoor experiment since these two parameters are related. The chemistry of the deliquescence process affected by the temperature changes and other factors that influences the long-term deliquescence will be further investigated in our future work.

A Mars analogous field-site operation of BOTTLE was also performed during the MINAR-5/NASA Spaceward Bound 2017 campaign at the Boulby mine, U.K, where samples from brine pool was used to demonstrate the instrument's ability to operate in Mars analogue environment [57]. During its operation on Mars, BOTTLE might pose some abnormal initial conditions such as improper salt distribution due to launch/landing operations or inclination in the platform that would allow the salts to slide towards the lower side and thus not maintaining the uniform depth of salts in each cell. These might be the possible sources that would hinder proper measurements over time at the beginning of the operation on Mars. This may render difficultly to precisely estimate the time of the first deliquescence as this requires a path between the electrodes. In case of a significant tilt, only once a sufficient amount of liquid brine is formed this path will be formed. To interpret the observations, if such a case arises while on Mars, we plan to make additional calibration with respect to inclination.

4.3. Water yield experiments

These outdoor experiments provided us a quantitative estimation of the amount of liquid brine that could be formed from a known amount of $CaCl_2$ and regolith-$CaCl_2$ samples. The sample of 1.2 g of anhydrous $CaCl_2$ (see Fig. 8) exposed to the arctic climatic conditions during December 2017, yielding up to 3.7 g of water in 3 days through deliquescence in an environment with temperature between 268.16 K and 273.16 K and relative humidity between 68% and 88%. We plan to carry 2 g of anhydrous $CaCl_2$ to Mars during the ExoMars launch in 2020, that will cover until the middle electrode of the BOTTLE cell. We chose to fill up the salts to this level based on our experience from calibration and outdoor experiment results (see section 4.1 and 4.2) to better characterize the water penetrating the salt during the brine formation process. This configuration also allows to restrict the maximum volume of brine formed in the most favourable environment conditions within the cell. This figure also illustrates visually the change in volume from dry salt matrix to liquid, and the redistribution of the brine.

We also observed a direct deliquescence process (see Fig. 9) in the other sample with a mixture of 1.2 g Mars regolith and 20% anhydrous $CaCl_2$ (0.3 g) when exposed to the outdoor climatic conditions. It took three days of exposure to the atmospheric moisture to enable the salt-regolith mixture to capture up to 1.025 g of water in an environment with low temperature (271.16 K) and high relative humidity (88%). Then we placed the petri dish in a laboratory environment at a temperature of 295.16 K and relative humidity varying from 7% to 22%, where we observed the sample turning into crystalline solids.

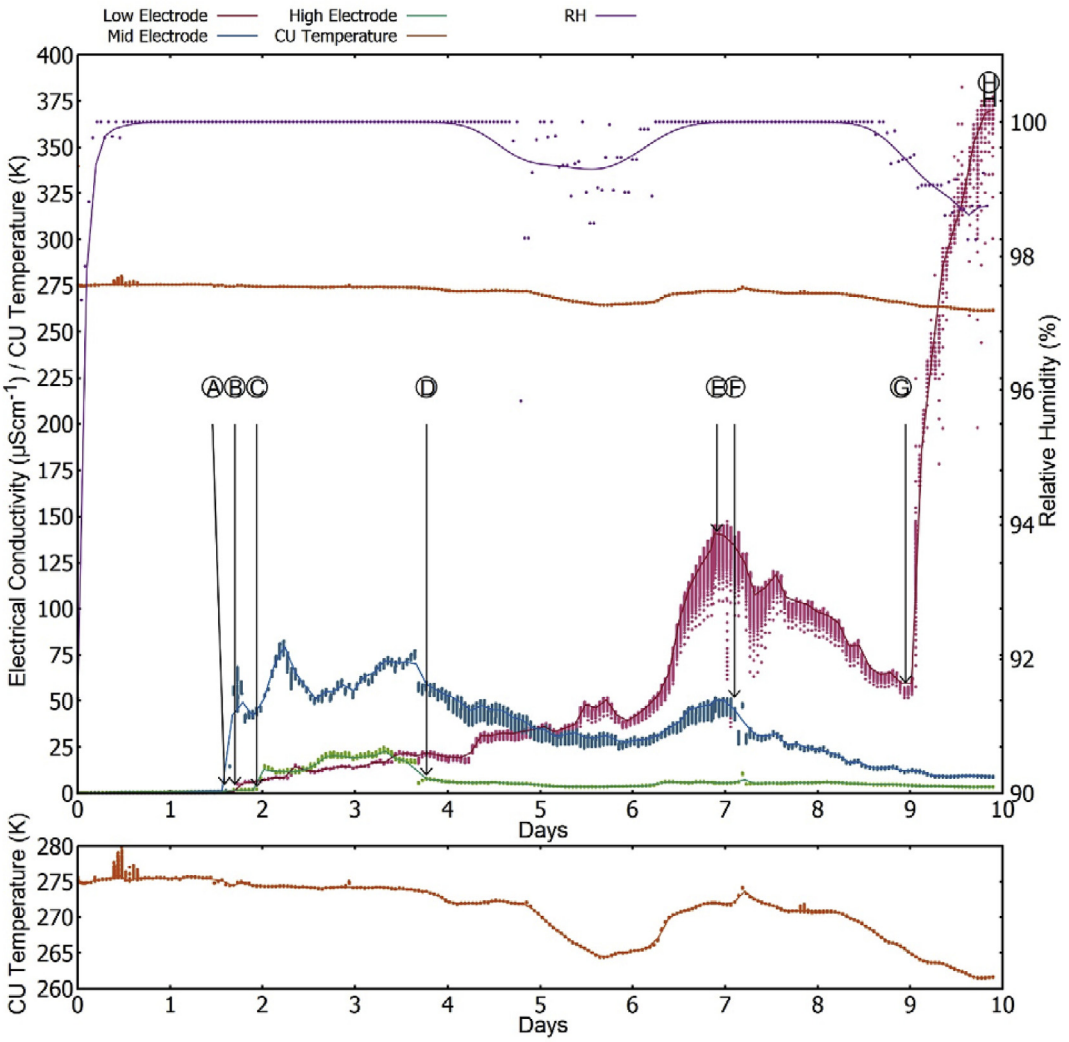

Fig. 7. Liquid brine formation process. A detailed account of Cell-5 of BOTTLE/HABIT data during the outdoor operation demonstration in Luleå, Sweden. The circled alphabets from 'A' through 'H' represent different stages of the observed brine formation process. The temperature (in left Y-axis) and relative humidity (in right Y-axis) are provided to support the context of the experiment. The temperature information is also provided as a subplot with a better scale.

Table 3
Summary of outdoor experiment progress.

Transition Point	Experiment state	Time
Start	Dry anhydrous $CaCl_2$ until mid-electrode	0
A	Deliquescence in the upper surface of the salt detected by mid electrode	38 h–1.6 d
B	Penetration of water into the salt detected by low electrode	40 h–1.7 d
C	Accumulation of brine pool in upper surface detected by high electrode	46 h–1.9 d
D	Brine hydrates shrinkage and lowering below high electrode	87 h–3.7 d
E	Brine hydrates lowering below mid electrode detected by low electrode	168 h–7 d
F	Brine hydrates lowering below mid electrode	172 h–7.2 d
G	Brine freezing detected by low electrode	214 h–9 d
H	End of experiment as brine freezing continued	237 h–9.9 d

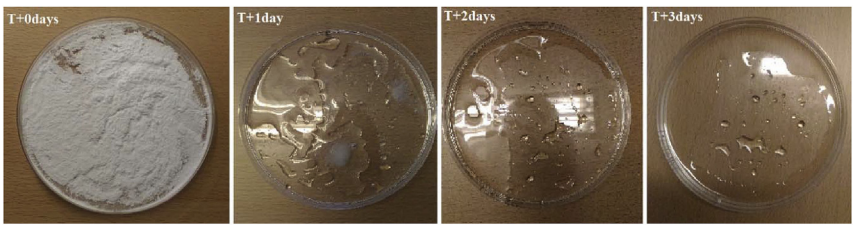

Fig. 8. Left to Right: Deliquescence process observed in 1.2 g anhydrous $CaCl_2$ from T + 0 days to T + 3 days. Images were taken at noon each day.

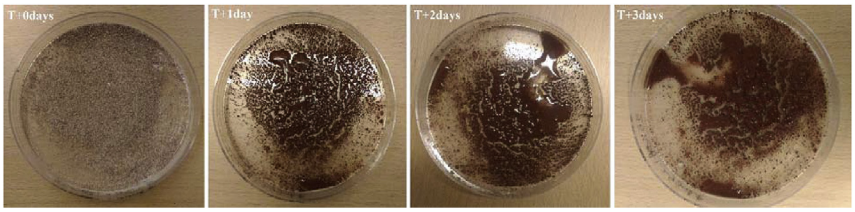

Fig. 9. Left to Right: Deliquescence process observed for a mixture of 1.2 g Mars regolith simulant and 0.3 g anhydrous $CaCl_2$ from T + 0 days to T + 3 days. All the images were taken at noon. The mixture at T + 0 days was in a dry granular form which turned into a thick slurry mixture on T + 1 day after absorbing some water from the atmosphere just enough to wet the regolith. At T + 2 days, due to the excess water intake, the slurry became loose with signs of the excess water flowing out to the corners of the petri dish. At T + 3 days, more water was absorbed.

4.4. Forced brine dehydration

The BOTTLE/HABIT engineering model has an in-built 5.5 W (100% duty cycle) heater (will be boosted to 12 W at 100% duty cycle in the flight model), for the purpose to: 1) recycle the liquid brine to anhydrous salt after the brine formation process, and 2) reset the instrument for detecting any degradation in the hardware and correct the offsets.

Our laboratory tests performed at ambient temperatures show that the empty CU could reach a maximum temperature of 333.85 K after heating for 2508 s and to a maximum temperature of 326.1 K with tap water in the CU after heating for 5737 s. Furthermore, dehydration of saturated calcium-chloride brine was performed in aluminium containers identical to CU, on a hot pot maintained at 328.15 K in the ambient laboratory environment. We found that it took about 7200 s to dehydrate the salt to its anhydrous form at Earth pressure. The temperature range for heating the salt was restricted around 328.15 K to avoid the brine from splashing away and to ensure retaining the original form of the salt to be able to reinitiate the brine formation process. Future BOTTLE tests will take place in a dedicated Martian simulation chamber, to determine the required duration of heating to release a given amount of captured water in the brine at Martian pressures.

This dehydration procedure will be carried out on Mars as a part of HABIT operation. This will serve to demonstrate the ISRU nature of the instrument as an in-situ resource utilization instrument to collect water for the future exploration of Mars.

5. Future plans

The results presented in this paper were implemented to present the BOTTLE calibration plan. We performed all the experiments described in this study using calcium-chloride. Future experiments are planned to study the relation between electrical conductivity, temperature and hydrate form for the other BOTTLE salts and under Martian conditions of pressure, temperature and relative humidity, in the Space Qualification (SpaceQ) chamber of the Luleå University of Technology. The present design of the HABIT instrument also considers other hygroscopic salts present on Mars such as sulphates. The final salt configuration will be chosen depending on the ability of the salt to retain its natural form after sterilisation procedures and bioburden analysis for planetary protection purposes. Another limiting factor to choose the final experimental salts to be stored in BOTTLE will be the long-term storage in ambient conditions which may allow some salts to absorb water while stored on Earth. We will run more experiments to characterize the role of the inhomogeneity in the brine distribution that resulted in the difference in the range of EC values between samples prepared for calibration experiments and the brine formation process during the outdoor operation of HABIT. The role of the inclination of the platform on the operation of HABIT will also be investigated. We are also planning to perform additional tests to observe the long-term exposure of the electrodes to the salt or brine as well as the performance of the products within the BOTTLE containers with respect to thermal cycling.

The EC measurements acquired on Mars will be used to determine the phase state of the salt as brine, hydrate, frozen or dehydrated state. The sudden changes in temperature measurements and EC values will be used to confirm the moment of phase state changes. However, for the case of hydrates, a complete assignment of the most dominant hydration state (i.e. for instance differentiating between tetra and hexahydrate) can only be achieved by: 1) comparing the phase diagrams with the T measurements provided by HABIT and the RH measurements provided by the environmental package of the IKI Surface Platform and 2) confirming with the Flight Model spare of HABIT in experimental simulations in the SpaceQ chamber of LTU (a simulation chamber which can operate at Martian atmospheric conditions, where pressure, T and RH are monitored and HABIT can provide measurements in real time), the state of the salts under equivalent pressure, T and RH conditions that lead to the same EC value.

The results expected under Martian conditions are similar to what has been shown here. Although on Mars the total water vapor present in the atmosphere is much lower than that on Earth, what is relevant for the phase state changes of the salts are the ambient T and RH. The existing water vapor on Mars is enough to hydrate or melt this amount of salts into liquid. In particular, taking for instance as reference the water vapor measured at Gale by the Curiosity Rover, there are up to 16 g of water available per night per m^2 [33]. Which means that the four salt containers of HABIT will most probably act as a water sink absorbing the water within an area of 1 m^2 around the instrument. Some previous experiments with salts under Martian simulated conditions have demonstrated these transitions on salts through visual images and IR spectroscopy [15]. After delivery of the Flight Model for integration on ExoMars, a dedicated campaign will be devoted to reproducing the expected operational conditions in the Mars simulation chamber. These experiments will demonstrate the expected changes of the EC caused by the simulated diurnal and seasonal changes predicted for the ExoMars landing site, at Oxia Planum.

6. Conclusions and Martian implications

The calibration procedure of BOTTLE/HABIT can be summarized into two main steps: i) converting the measured current flow, I and the voltage drop, V across the total of 16 electrode pairs to actual electrical conductivity by applying geometrical cell constants and the two-point calibration function, and ii) providing the context to the electrical conductivity measurements in terms of temperature and salt hydration form to determine the phase of brine formed.

This work provides a fresh insight to the world of observing the brine formation process which were previously studied predominantly using techniques [16–19,42,58] such as Raman microscope, optical visual images, particle levitation experiments, which has limitations in identifying the phase transitions in bulk samples and demand complex sample preparation techniques, experimental setup and operational requirements. On the other hand, the EC technique provides substantial characterization of the liquid brine formation and its phase transitions while being robust, simple to operate, and adequate to be embedded into a small mass, power and volume, durable, low cost and maintenance instrument such as HABIT.

The clear detection of an EC change in BOTTLE after commissioning the instrument on Mars would reveal that the deliquescence mechanism is in effect on Mars. This would have many major implications. First, it would confirm the possibility of a present day atmosphere-regolith

interaction that may lead to the formation of briny mixtures of soil as those shown in Fig. 9. These briny mixtures with soil, in the case of deep slopes may be observed from orbit through large-scale features like RSL. The identification of the transient liquid water and its stability time scales would open the discussion about the possibility of life in present day Mars and various other key points linked with the future human exploration. It is also expected that the demonstration of the formation of liquid brine would have implications on the definition of special regions defined for planetary protection purposes. Finally, this technology will help to demonstrate the possibility of in-situ water harvesting for future human and robotic missions to Mars.

Acknowledgements

The authors thank Alvaro Soria-Salinas and Thasshwin Mathanlal for assisting with and monitoring the outdoor operation demonstration. The HABIT Engineering Model was fabricated by Omnisys, Sweden, as part of the HABIT project development and funded by the Swedish National Space Agency (SNSA). We would like to thank the Kempe foundation for its generous funding support. This project also received a seed funding from the Dubai Future Foundation through Guaana.com open research platform (https://www.guaana.com/projects/jeGEimuX6DLCLsbQP).

Nomenclature

σ_{actual}	Actual electrical conductivity
G	Conductance
I	Current
Σ	Electrical conductivity
K_{cell}	Geometrical cell constant
W	Mass fraction
$\sigma_{measured}$	Measured electrical conductivity
μScm^{-1}	Micro siemens per centimetre
x	Mole fraction
RH	Relative humidity
S	Siemens
T	Temperature
V	Voltage
wt%	Weight percent

Appendix B. Supplementary data

Supplementary data to this article can be found online at https://doi.org/10.1016/j.actaastro.2019.06.026.

Conflicts of interest

The authors declare no competing interests.

References

[1] C.S. Cockell, et al., Habitability: A Review 16 (1) (2016) 89–117 https://doi.org/10.1089/ast.2015.1295.
[2] Viscio, et al., A methodology to support strategic decisions in future human space exploration: from scenario definition to building blocks assessment, Acta Astronaut. 91 (2013) 198–217 https://doi.org/10.1016/j.actaastro.2013.06.015.
[3] DeVincenzi, et al., Planetary protection, sample return missions and Mars exploration: history, status, and future needs, J. Geophys. Res. 103 (E12) (1998) 28577–28586 https://doi.org/10.1029/98JE01600.
[4] J. Martín-Torres, M.-P. Zorzano, Should we invest in martian brine research to reduce Mars exploration costs? Astrobiology 17 (1) (2017) 3–7 https://doi.org/10.1089/ast.2016.1602.
[5] M.H. Hecht, S.P. Kounaves, R.C. Quinn, S.J. West, S.M.M. Young, D.W. Ming, D.C. Catling, B.C. Clark, W.V. Boynton, J. Hoffman, L.P. DeFlores, K. Gospodinova, J. Kapit, P.H. Smith, Detection of perchlorate and the soluble chemistry of martian soil at the Phoenix lander site, Science 325 (2009) 64–67 https://doi.org/10.1126/science.1172466.
[6] L. Leshin, P.R. Mahaffy, C.R. Webster, M. Cabane, P. Coll, P.G. Conrad, P.D. Archer Jr., S.K. Atreya, A.E. Brunner, A. Buch, J.L. Eigenbrode, G.J. Flesch, H.B. Franz, C. Freissinet, D.P. Glavin, A.C. McAdam, K.E. Miller, D.W. Ming, R.V. Morris, R. Navarro-González, P.B. Niles, T. Owen, R.O. Pepin, S. Squyres, A. Steele, J.C. Stern, R.E. Summons, D.Y. Sumner, B. Sutter, C. Szopa, S. Teinturier, M.G. Trainer, J.J. Wray, J.P. GrotzingerMSL Science Team, Volatile, isotope and organic analysis of martian fines with the Mars Curiosity Rover, Science 341 (2013), https://doi.org/10.1126/science.1238937.
[7] D.P. Glavin, et al., Evidence for perchlorates and the origin of chlorinated hydrocarbons detected by SAM at the Rocknest aeolian deposit in Gale Crater, J. Geophys. Res. Planets 118 (10) (2013) 1955–1973 https://doi.org/10.1002/jgre.20144.
[8] D.W. Ming, P.D. Archer Jr., D.P. Glavin, J.L. Eigenbrode, H.B. Franz, B. Sutter, A.E. Brunner, J.C. Stern, C. Freissinet, A.C. McAdam, P.R. Mahaffy, M. Cabane, P. Coll, J.L. Campbell, S.K. Atreya, P.B. Niles, J.F. Bell III, D.L. Bish, W.B. Brinckerhoff, A. Buch, P.G. Conrad, D.J. Des Marais, B.L. Ehlmann, A.G. Fairén, K. Farley, G.J. Flesch, P. Francois, R. Gellert, J.A. Grant, J.P. Grotzinger, S. Gupta, K.E. Herkenhoff, J.A. Hurowitz, L.A. Leshin, K.W. Lewis, S.M. McLennan, K.E. Miller, J. Moersch, R.V. Morris, R. Navarro-González, A.A. Pavlov, G.M. Perrett, I. Pradler, S.W. Squyres, R.E. Summons, A. Steele, E.M. Stolper, D.Y. Sumner, C. Szopa, S. Teinturier, M.G. Trainer, A.H. Treiman, D.T. Vaniman, A.R. Vasavada, C.R. Webster, J.J. Wray, R.A. YingstMSL Science Team, Volatile and organic compositions of sedimentary rocks in Yellowknife Bay, Gale Crater, Mars, Science 343 (2014), https://doi.org/10.1126/science.1245267.
[9] R. Navarro-González, et al., Reanalysis of the Viking results suggests per-chlorate and organics at midlatitudes on Mars, J. Geophys. Res. Planets 115 (2010), https://doi.org/10.1029/2010JE003599.
[10] M.M. Osterloo, F.S. Anderson, V.E. Hamilton, B.M. Hynek, Geologic context of proposed chloride-bearing materials on Mars, J. Geophys. Res. 115 (2010) E02010 https://doi.org/10.1029/2010JE003613.
[11] J.M. Keller, W.V. Boynton, S. Karunatillake, V.R. Baker, J.M. Dohm, L.G. Evans, M.J. Finch, B.C. Hahn, D.K. Hamara, D.M. Janes, K.E. Kerry, H.E. Newsom, R.C. Reedy, A.L. Sprague, S.W. Squyres, R.D. Starr, G.J. Taylor, R.M.S. Williams, Equatorial and midlatitude distribution of chlorine measured by Mars Odyssey GRS, J. Geophys. Res. 111 (2006), https://doi.org/10.1029/2006JE002679.
[12] W.C. Feldman, T.H. Prettyman, S. Maurice, J.J. Plaut, D.L. Bish, D.T. Vaniman, M.T. Mellon, A.E. Metzger, S.W. Squyres, S. Karunatillake, W.V. Boynton, R.C. Elphic, H.O. Funsten, D.J. Lawrence, R.L. Tokar, Global distribution of near-surface hydrogen on Mars, J. Geophys. Res. 109 (2004) E09006 https://doi.org/10.1029/2003JE002160.
[13] Zhongchen Wu, et al., Forming perchlorates on Mars through plasma chemistry during dust events, Earth Planet. Sci. Lett. 504 (2018) 94–105 https://doi.org/10.1016/j.epsl.2018.08.040.
[14] V. Chevrier, J. Hanley, T. Altheide, Stability of perchlorate hydrates and their liquid solutions at the Phoenix landing site, Mars, Geophys. Res. Lett. 36 (2009) L10202 https://doi.org/10.1029/2009GL037497.
[15] M.-P. Zorzano, E. Mateo-Martí, O. Prieto-Ballesteros, S. Osuna, N. Renno, Stability of liquid saline water on present day Mars, Geophys. Res. Lett. 36 (2009) L20201 https://doi.org/10.1029/2009GL040315.
[16] R.V. Gough, V.F. Chevrier, K.J. Baustian, M.E. Wise, M.A. Tolbert, Laboratory studies of perchlorate phase transitions: support for metastable aqueous perchlorate solutions on Mars, Earth Planet. Sci. Lett. 312 (3–4) (2011) 371–377 https://doi.org/10.1016/j.epsl.2011.10.026.
[17] R.V. Gough, V.F. Chevrier, M.A. Tolbert, Formation of aqueous solutions on Mars via deliquescence of chloride-perchlorate binary mixtures, Earth Planet. Sci. Lett. 393 (2014) 73–82 https://doi.org/10.1016/j.epsl.2014.02.002.
[18] R.V. Gough, V.F. Chevrier, M.A. Tolbert, Formation of liquid water at low temperatures via the deliquescence of calcium chloride: implications for Antarctica and Mars, Planet. Space Sci. 131 (2016) 79–87 https://doi.org/10.1016/j.pss.2016.07.006.
[19] E. Fischer, G.M. Martínez, H.M. Elliott, N.O. Rennó, Experimental evidence for the formation of liquid saline water on Mars, Geophys. Res. Lett. 41 (2014) 4456–4462 https://doi.org/10.1002/2014GL060302.
[20] D.L. Nuding, E.G. Rivera-Valentin, R.D. Davis, R.V. Gough, V.F. Chevrier, M.A. Tolbert, Deliquescence and efflorescence of calcium perchlorate: an investigation of stable aqueous solutions relevant to Mars, Icarus 243 (2014) 420–428 https://doi.org/10.1016/j.icarus.2014.08.036.
[21] D.L. Nuding, R.D. Davis, R.V. Gough, M.A. Tolbert, The aqueous stability of a Mars salt analog: instant Mars, J. Geophys. Res. Planets 120 (2015) 588–598 https://doi.org/10.1002/2014JE004722.
[22] G. Nikolakakos, J.A. Whiteway, Laboratory investigation of perchlorate deliquescence at the surface of Mars with a Raman scattering lidar, Geophys. Res. Lett. 42 (2015) 7899–7906 https://doi.org/10.1002/2015GL065434.
[23] M. Chojnacki, A. McEwen, C. Dundas, L. Ojha, A. Urso, S. Sutton, Geologic context of recurring slope lineae in melas and coprates chasmata, Mars, J. Geophys. Res. Planets 121 (2016) 1204–1231 https://doi.org/10.1002/2015JE004991.
[24] A. McEwen, et al., Seasonal flows on warm martian slopes, Science (New York, NY) 333 (6043) (2011) 740–743 https://doi.org/10.1126/science.1204816.
[25] A.S. McEwen, et al., Recurring slope lineae in equatorial regions of Mars, Nat. Geosci. 7 (1) (2014) 53–58 https://doi.org/10.1038/ngeo2014.
[26] A. McEwen, M. Chojnacki, C. Dundas, L. Ojha, M. Masse, E. Schaefer, C. Leung, Recurring slope lineae on Mars: atmospheric origin? EPSC Abstracts 10 (2015) EPSC2015-E2786-1.
[27] K. Runyon, L. Ojha, Recurring slope lineae, in: H. Hargitai, Á. Kereszturi, pages (Eds.), Encyclopedia of Planetary Landforms, Springer, New York, 2014, pp. 1–6 https://doi.org/10.1007/978-1-4614-9213-9_352-1.
[28] V.F. Chevrier, E.G. Rivera-Valentin, Formation of recurring slope lineae by liquid brines on present-day Mars, Geophys. Res. Lett. 39 (21) (2012) L21202.
[29] L. Ojha, M.B. Wilhelm, S.L. Murchie, A.S. McEwen, J.J. Wray, J. Hanley, M. Massé,

M. Chojnacki, Spectral evidence for hydrated salts in recurring slope lineae on Mars, Nat. Geosci. 8 (2015) 829–832 https://doi.org/10.1029/2012GL054119.
[30] A. Bhardwaj, L. Sam, F.J. Martín-Torres, M.-P. Zorzano, R.M. Fonseca, Martian slope streaks as plausible indicators of transient water activity, Sci. Rep. 7 (2017) 7074 https://doi.org/10.1038/s41598-017-07453-9.
[31] Mikhail A. Kreslavsky, James W. Head, Slope streaks on Mars: a new "wet" mechanism, Icarus 201 (2) (2009) 517–527 https://doi.org/10.1016/j.icarus.2009.01.026.
[32] A. Kereszturi, E.G. Rivera-Valentin, Possible water lubricated grain movement in the circumpolar region of Mars, Planet. Space Sci. 125 (2016) 130–146 https://doi.org/10.1016/j.pss.2016.03.015.
[33] Martín-Torres, et al., Transient liquid water and water activity at Gale crater on Mars, Nat. Geosci. 8 (2015) 357–361 https://doi.org/10.1038/ngeo2412.
[34] B. Pál, Á. Kereszturi, Possibility of microscopic liquid water formation at landing sites on Mars and their observational potential, Icarus 282 (2017) 84–92 https://doi.org/10.1016/j.icarus.2016.09.006.
[35] Rivera-Valentín, et al., Constraining the potential liquid water environment at Gale Crater, Mars, J. Geophys. Res.: Planets 123 (5) (2018) 1156–1167 https://doi.org/10.1002/2018JE005558.
[36] A. Kereszturi, G. Sandor, Possibility of H_2O_2 decomposition in thin liquid films on Mars, Planet. Space Sci. 103 (2014) 153–166 https://doi.org/10.1016/j.pss.2014.07.017.
[37] Domagal-Goldman, D. Shawn, et al., The astrobiology primer v2.0, Astrobiology 16 (8) (2016) 561–653 https://doi.org/10.1089/ast.2015.1460.
[38] S.T. Martin, Phase transitions of aqueous atmospheric particles, Chem. Rev. 100 (9) (2000) 3403–3454 https://doi.org/10.1021/cr990034t.
[39] A.F. Davila, et al., Hygroscopic salts and the potential for life on Mars, Astrobiology 10 (6) (2010) 617–628 https://doi.org/10.1089/ast.2009.0421.
[40] J. Heinz, D. Schulze-Makuch, S.P. Kounaves, Deliquescence induced wetting and RSL-like darkening of a Mars analogue soil containing various perchlorate and chloride salts, Geophys. Res. Lett. 43 (2016) 4880–4884 https://doi.org/10.1002/2016GL068919.
[41] D.R. Lide, CRC Handbook of Chemistry and Physics: A Ready-Reference Book of Chemical and Physical Data, 84th ed., CRC Press, Boca Raton, Fla, 2003.
[42] R.V. Gough, J. Wong, J.L. Dickson, J.S. Levy, J.W. Head, D.R. Marchant, M.A. Tolbert, Brine formation via deliquescence by salts found near Don Juan Pond, Antarctica: laboratory experiments and field observational results, Earth Planet. Sci. Lett. 476 (2017) 189–198 https://doi.org/10.1016/j.epsl.2017.08.003.
[43] J.D. Toner, D.C. Catling, the formation of liquid water on present-day Mars: calcium-magnesium chloride brines in the antarctic dry Valleys as a Mars analog, The Sixth International Conference on Mars polar science and exploration, Reykjavik, Iceland, 2016, pp. 5–9 September.
[44] J.H. Seinfeld, S.N. Pandis, Atmospheric Chemistry and Physics: from Air Pollution to Climate Change, second ed., John Wiley and Sons, Inc., New York, NY, 1998.
[45] R.D. Davis, et al., Contact efflorescence as a pathway for crystallization of atmospherically relevant particles, Proc. Natl. Acad. Sci. USA112 (52) (2015) 15815–15820 https://doi.org/10.1073/pnas.1522860113.
[46] I. Tang, Thermodynamic and optical properties of mixed-salt aerosols of atmospheric importance, J. Geophys. Res. 102 (D2) (1997) 1883–1893 https://doi.org/10.1029/96JD03085.
[47] Jaroslav Patek, Jaroslav Klomfar, Monika Souckova, Solid-liquid equilibrium in the system of CaCl2-H2O with special regard to the transition points, J. Chem. Eng. Data 53 (2008) 2260–2271 https://doi.org/10.1021/je800009w.
[48] J. Baustian, M.E. Wise, M.A. Tolbert, Depositional ice nucleation on solid ammonium sulfate and glutaric acid particles, Atmos. Chem. Phys. 10 (5) (2010) 2307–2317 https://doi.org/10.5194/acp-10-2307-2010.
[49] K.M. Primm, Freezing of perchlorate and chloride brines under Mars-relevant conditions, Geochem. Cosmochim. Acta 212 (2017) 211–220 https://doi.org/10.1016/j.gca.2017.06.012.
[50] K.M. Primm, The effect of mars-relevant soil analogs on the water uptake of magnesium perchlorate and implications for the near-surface of Mars, J. Geophys. Res.: Planets 123 (8) (2018) 2076–2088 https://doi.org/10.1029/2018JE005540.
[51] J.D. Toner, The formation of supercooled brines, viscous liquids, and low-temperature perchlorate glasses in aqueous solutions relevant to Mars, Icarus 233 (2014) 36–47 https://doi.org/10.1016/j.icarus.2014.01.018.
[52] G. Nikolakakos, J.A. Whiteway, Laboratory studies of perchlorate deliquescence and water adsorption at the surface of Mars, Icarus 308 (2018) 221–229 https://doi.org/10.1016/j.icarus.2017.05.006.
[53] C.P. McKay, E.I. Friedmann, B. Gómez-Silva, L. Cáceres-Villanueva, D.T. Andersen, R. Landheim, Temperature and moisture conditions for life in the extreme arid region of the Atacama desert: four years of observations including the El Niño of 1997–1998, Astrobiology 3 (2) (2003) 393–406 https://doi.org/10.1089/153110703769016460.
[54] W.L. Davis, I. de Pater, C.P. McKay, Rain infiltration and crust formation in the extreme arid zone of the Atacama Desert, Chile, Planet, Space Sci. 58 (4) (2010) 616–622 https://doi.org/10.1016/j.pss.2009.08.011.
[55] R.C. Weast (Ed.), CRC Handbook of Chemistry, and Physics, 70th Edition, CRC Press, Boca Raton, FL, 1989, p. 221.
[56] A.V. Wolf, Aqueous Solutions and Body Fluids, Harper and Row, New York, 1966.
[57] C.S. Cockell, et al., Subsurface scientific exploration of extraterrestrial environments (MINAR 5): analogue science, technology and education in the Boulby Mine, UK, Int. J. Astrobiol. 11 (12) (2018) 21 https://doi.org/10.1017/S1473550418000186.
[58] E. Fischer, Searching for brine on Mars using Raman spectroscopy, Física Tierra 28 (2016) 181–195 http://doi.org/10.5209/rev_FITE.2016.v28.53903.